Water Research 284 (2025) 123981

Contents lists available at ScienceDirect

Water Research

journal homepage: www.elsevier.com/locate/watres

Formation of highly toxic halogenated coupling byproducts in UV/Chlorine reaction of phenols in presence of halides

Mengge Fan [a], Yangjian Zhou [a], Jialing Luo [b], Yanpeng Gao [b], Junlang Qiu [a,*], Xin Yang [a]

[a] School of Environmental Science and Engineering, Guangdong Provincial Key Laboratory of Environmental Pollution Control and Remediation Technology, Sun Yat-sen University, Guangzhou, 510275, China
[b] Guangdong Key Laboratory of Environmental Catalysis and Health Risk Control, Guangzhou Key Laboratory Environmental Catalysis and Pollution Control, School of Environmental Science and Engineering, Institute of Environmental Health and Pollution Control, Guangdong University of Technology, Guangzhou 510006, China

ARTICLE INFO

Keywords:
UV/Chlorine
Disinfection byproducts
Bromide
Effect-directed analysis
Halogenated coupling byproducts
toxicity

ABSTRACT

With drinking water disinfection techniques evolving from chlorination/chloramination to advanced oxidation processes, the conundrum of disinfection byproducts (DBPs) formation that remains for decades is becoming more challenging. This study focuses on the formation of unknown halogenated coupling byproducts, an important class of DBPs neglected in previous investigations, from UV/Chlorine reaction of phenols in presence of halides. To prioritize the highly toxic compounds, the effect-directed analysis strategy involving nontargeted identification with high-resolution mass spectrometry was utilized. The presence of bromide was found to enhance the formation of known DBPs, total organic halogens, and the overall toxicity of treated water. In contrast, iodide at environmentally relevant concentration exhibited minimal effects on the DBP formation and toxicity. Assisted with density functional theory calculation, a series of halogenated coupling byproducts were identified in the reaction involving bromide. The formation mechanisms of halogenated coupling byproducts consist of halogen substitution, free-radical-mediated electron transfer, hydroxylation, among others. As indicated by computational toxicity evaluation, these halogenated coupling byproducts were surprisingly harmful in human thyroperoxidase activity inhibition and aquatic toxicity. This study provides new insights into the DBP formation during UV/Chlorine reaction, and the findings unveiled the emergence of highly toxic halogenated coupling byproducts especially in presence of halides.

1. Introduction

Disinfection has been implemented in drinking water treatment for over a century to eliminate pathogenic bacteria and ensure water safety (Li and Mitch, 2018). However, the use of disinfectants can lead to the formation of toxic disinfection byproducts (DBPs) (Allen et al., 2022b; Jiang et al., 2025). Chlorine, the most widely used disinfectant, can react with organics in source water to form chlorinated DBPs (Cl-DBPs) such as trichloromethane (TCM) and chlorinated acetic acids (Qian et al., 2021). These DBPs have been regulated due to their cytotoxicity, mutagenicity, teratogenicity and carcinogenicity (Alexandrou et al., 2018; Allen et al., 2022a; Srivastav et al., 2020). The natural organic matter (NOM) featuring phenolic groups (10 %−30 %) in source water represents the primary precursor of DBPs (Lavonen et al., 2013; Watson et al., 2018; Li et al., 2019), and the inorganic halides (i.e., bromide (Br^-) and iodide (I^-)) can also influence the speciation of DBPs (Liu et al., 2019, 2022, 2018). The presence of Br^- and I^- has been found to result in the formation of brominated DBPs (Br-DBPs) and iodinated DBPs (I-DBPs), which are generally more toxic than Cl-DBPs (Liu et al., 2017; Wang et al., 2014; Yang et al., 2014).

In recent years, UV irradiation and chlorine have been used in combination as an advanced oxidation process, i.e., UV/Chlorine, for water disinfection. UV/Chlorine reaction can generate hydroxyl radical ($HO^•$) and chlorine radicals ($Cl^•$, $ClO^•$, and $Cl_2^{•-}$) (Cheng et al., 2018; Kong et al., 2023) to initiate a variety of chemical reactions. These reactions are not only effective in elimination of diverse emerging contaminants such as phenols and amines (Fan et al., 2022; Lei et al., 2019), but also achieve inactivation of pathogenic microorganisms by damaging their membrane, enzymes, DNA, and RNA (Chen et al., 2021). Nevertheless, the presence of NOM in source water can decrease the elimination efficiency of UV/Chlorine treatment for contaminants, compromise the pathogen inactivation capacity, and lead to the

* Corresponding author.
E-mail address: qiujlang@mail.sysu.edu.cn (J. Qiu).

https://doi.org/10.1016/j.watres.2025.123981
Received 13 February 2025; Received in revised form 5 June 2025; Accepted 6 June 2025
Available online 12 June 2025

formation of harmful DBPs (Yeom et al., 2021). A series of typical DBPs including trihalomethanes (THMs) and haloacetic acid (HAAs) have been detected during UV/Chlorine reaction (Bulman et al., 2023). Moreover, the increase of HAA formation and total organic halogen has been observed, which would be ascribed to the highly reactive chlorine species (RCS) generated in UV/Chlorine reaction (Lei et al., 2021; Wang et al., 2017). On the other hand, the presence of halides in source water would participate in the DBP formation during UV/Chlorine reaction. Specifically, Br^- leads to the formation of $HOBr/BrO^-$ and reactive bromine species (RBS) (e.g., $Br^•$, $BrO^•$, $Br_2^{•-}$, $BrOH^{•-}$ and $ClBr^{•-}$) (Cheng et al., 2018; Zhang et al., 2020), which decreased the formation of Cl-DBPs but increased the formation of Br-DBPs in UV/Chlorine reaction (Dong et al., 2021; Huang et al., 2022). The formation of RBS occurs through two distinct pathways: (i) the reaction of RCS with Br^-, and (ii) the photolytic decomposition of HOBr. These generated RBS subsequently participate in the degradation of organic pollutants via either single electron transfer or addition reactions (Lei et al., 2022). While the presence of I^- also alters the formation of DBPs in UV/Chlorine reaction by generating HOI/IO^- and reactive iodine species (RIS) (Gao et al., 2020; Ye et al., 2021). Similar to RBS, RIS are generated through two primary mechanisms: (i) the oxidation of I^- by RCS, and (ii) the photolytic decomposition of HOI. The resultant RIS subsequently participate in organic pollutant degradation through single electron transfer mechanisms, similar to their brominated counterparts. (Yang et al., 2025). For example, a 10 μM I^- in UV/Chlorine reaction of humic acid was found to increase the yields of HAAs while slight decrease those of THMs (Gao et al., 2020).

Although research efforts have been made to clarify the DBP formation in UV/Chlorine reaction, the majority of DBP species remains unknown. >60 % of the total organic halogen (TOX) generated in UV/Chlorine reaction cannot be explained by the identified DBPs (Zhao et al., 2023). Meanwhile, toxicity evaluation revealed that the unknown DBPs produced in advanced oxidation processes (AOPs) were important toxicity contributors, emphasizing the significance to ascertain the unknown DBPs in UV/Chlorine reaction (Chen et al., 2025). Recently, high-molecule-weight DBPs, which contain more than two carbon atoms (Mitch et al., 2023), have been identified in drinking water disinfection with conventional techniques such as chlorination and chloramination, which opened up a new area in the catalogue of DBPs. Similarly, a series of high-molecule-weight products, such as coupling compounds like the dimer of diallyl phthalate with a molecular weight of 521.15 and the dimer of diethyl phthalate with a molecular weight of 473.15, were found in AOPs of micropollutants in water (Chen et al., 2024; Zhang et al., 2024, 2023; Zheng et al., 2023). More importantly, these high-molecule-weight products generally showed higher toxicity compared to the precursors as well as the common low-molecule-weight products, implying for potential toxicity contributors in the treated water of AOPs. Given the superior reactivity nature of UV/Chlorine reaction, it is reasonable to expect the formation of high-molecule-weight products in its application for drinking water disinfection. However, the complexity of NOM leads to the formation of various DBPs in UV/Chlorine reaction, rendering the identification of highly toxic high-molecule-weight DBPs an intractable task (Dong et al., 2023). Effect-directed analysis (EDA) can reduce the chemical complexity through bioassay-directed fractionation, which offers an effective tool to tackle the challenge (Brack, 2003; Brack et al., 2016; Dong et al., 2020). By integrating biological and chemical analyses, the methodology of EDA allows for prioritization of highly toxic portions in the overall products, drastically facilitating a more focused identification of unknown highly toxic high-molecule-weight DBPs in UV/Chlorine reaction.

This study aims to reveal the formation of highly toxic coupling DBPs in UV/Chlorine reaction of phenols in presence of halides. The EDA strategy was employed to fractionate and prioritize the DBPs with high toxicity, and the high-resolution mass spectrometry (HRMS) assisted with density functional theory (DFT) calculation was performed to elucidate the structure of unknown coupling DBPs. These coupling byproducts were confirmed in UV/Chlorine reaction of simulated source water containing NOM. To gain insights into the nature of coupling DBPs, the formation mechanisms were proposed based on the experimental observations of reactive species and the theoretical evidences from computation. Additionally, the potential toxicity of identified coupling DBPs were evaluated through ecological structure activity relationship modelling.

2. Materials and methods

2.1. Chemicals and reagents

The stock solution of free chlorine was prepared by diluting 5 % Sigma-Aldrich sodium hypochlorite (NaOCl) (the USA) to a concentration of 1000 mg L^{-1} as Cl_2. Standards of DBPs including six THMs, nine HAAs, seven haloacetaldehydes (HALs), and two internal standards (1,2-dibromopropane and 2,3-dibromopropionic acid) were obtained from Supelco (the USA). Sodium thiosulfate and other inorganic salts were purchased from Aladdin (China). All reagents used in this study were of reagent grade. The NOM stock solution was prepared by dissolving the International Humic Substances Society Cat. No.2R101N Suwannee River NOM (SRNOM) isolate (the USA) in water followed by filtering through a 0.45 μm glass fiber membrane. The detailed information regarding the other chemicals and reagents used in this study is presented in Text S1. *Photobacterium phosphoreum* T3 *(P. phosphoreum* T3*)* was supplied as freeze-dried powder by Jiachu Biological Engineering Co., LTD (China).

2.2. UV/Chlorine experiment

All tests were conducted in an airtight quartz vessel at a volume of 120 mL. The experimental solution contained phenol at a concentration of 10 μM was prepared with 5.0 mM phosphate buffer at pH 7.0. A collimated beam apparatus equipped with two UV lamps (8 W each) emitting at a wavelength of 253.7 nm was utilized for the UV treatment. A quartzose dish with a diameter of 7.5 cm was placed directly beneath the UV beam. The incident fluence rate was 0.27 mW cm^{-2} measured by KI-KIO_3 chemical actinometry (Bolton et al., 2011; Rahn, 1997).

To initiate the UV/Chlorine process, the solutions were subjected to UV irradiation and treated with 0.1 mM of Cl_2. The concentrations of Br^- and I^- in natural waters typically range from ~5–500 μg L^{-1} and 0.5–100 μg L^{-1}, respectively (Shimabuku et al., 2024; Mackeown et al., 2022). To simulate natural water conditions and systematically evaluate the impact of halide ions, the experimental concentrations of Br^- and I^- were selected to approximate the upper concentration ranges observed in environmental systems. Br^- and I^- were added to individual reaction solutions at concentrations of 0.5 mg L^{-1} and 0.1 mg L^{-1}, respectively. The radical probe nitrobenzene (NB, 20 μM) was spiked into the solution to quantify the $HO^•$ concentrations. At various time intervals (3–30 min), samples were collected, quenched with sodium thiosulfate, and subsequently analyzed to measure the probe concentrations using liquid chromatography. $HO^•$ concentrations were calculated by measuring the depletion of NB (details in Text S2). Due to the presence of halogen ions, the steady-state concentrations of the reactive halogen species (RHS), including $Cl^•$, $ClO^•$, $Cl_2^{•-}$, $Br^•$, $BrO^•$, $Br_2^{•-}$, and $ClBr^{•-}$, were obtained by using the Kintecus software (Version 5.55), following the methods reported in our previous study (Cheng et al., 2018). For the analysis of known DBPs and TOX formation, samples irradiated by a UV flux of 500 mJ cm^{-2} were quenched with ascorbic acid prior to instrumental analysis. All of the experiments were performed in triplicate to ensure data reproducibility and reliability. To simulate UV/Chlorine treatment under environmentally relevant conditions, an aqueous solution containing 5 mgC L^{-1} NOM buffered with 5 mM phosphate buffer at pH 7.0 was irradiated with UV light and treated with 0.1 mM of Cl_2. The treated water was then concentrated and analyzed by HRMS to characterize the

resulting halogenated coupling byproducts.

2.3. Analytical methods

2.3.1. Determination of known DBPs and TOX

A total of 22 halogenated DBPs, categorized into three DBP groups, were analyzed (Table S2). The liquid extraction procedures and analytical methods were modified based on USEPA Methods 551.1/552.3 and our previous study (Zhong et al., 2019). Details regarding the extraction methods were provided in Text S3 and the measurement of TOX, including total organic chlorine (TOCl), total organic chlorine (TOBr) and total organic iodine (TOI), were provided in Text S4.

2.3.2. Toxicity assessment of water samples

Each sample was concentrated by solid phase extraction (SPE) using CNW HLB cartridges (China), the details are described in Text S5. It should be noted that the SPE extraction and N_2 dry-up procedures result in the loss of most volatile DBPs, including THMs and HALs, as reported in the previous study (Zhong et al., 2019). Consequently, the toxicity tests conducted in this study indicated only the toxicity of less volatile DBPs. The acute toxicity of the samples was assessed using *P. phosphoreum* T3 following the national standard method of China, GB/T 15,441–1995. In brief, an aliquot of 10 μL of bacteria solution containing 400,000 cells per milliliter was spiked into 200 μL water sample concentrate that redissolved in 3 % NaCl solution. The details of toxicity assessment were provided in Text S6.

In order to further identify the toxic byproducts, the extracted samples were separated into fractions before toxicity analysis. Briefly, the water sample concentrates were fractionated on a Shimadzu LC20 high-performance liquid chromatograph (HPLC) (Japan) equipped with a Shimadzu Shim-pack PREP-ODS preparative reversed-phase C18 column (20 mm × 25 cm × 5 μm) (Japan). The binary mobile phase consisted of (A) water and (B) methanol, both containing 0.25 % formic acid. The HPLC operating conditions and elution programs are provided in Text S7. After sample injection, ten fractions were collected every 10 min with a fraction volume of 20 mL each. The collected fractions were concentrated by N_2 purging and freeze drying before diluted for toxicity analysis and mass spectrometry analysis.

To investigate the properties of compounds within each fraction, a set of halo-DBPs with varying LogKow values, including 6 aliphatic and 7 aromatic halo-DBPs, were selected and fractionated using the same preparative procedure. Based on the retention times (RTs) of the halo-DBPs, the dividing line for separating aliphatic and aromatic halo-DBPs was determined. As shown in Fig. S4, the dividing line was determined to be the RT of 40 min. In other words, the aliphatic fraction was likely to be collected in fraction1 (F1) − fraction4 (F4) with the RT range of 0 min to 40 min, while the aromatic fraction was supposed to be collected in F5−F10.

2.3.3. Detection of phenoxyl radicals

Two trapping agents, i.e., (2,2,6,6-tetramethylpiperidin-1-yl) oxyl (TEMPO)-based traps containing alkyl (CHANT) and TEMPO, were used to identify phenoxyl radicals in the UV/Chlorine reactions. A Waters ACQUITY I-Class ultra-performance liquid chromatograph coupled to a Waters Synapt G2-Si quadrupole time-of-flight mass spectrometer (UPLC-Q-TOF MS) (the USA) was applied to detect the phenoxyl radical capture adducts. The detailed information for the detection of phenoxyl radical capture adducts was provided in Text S8.

2.3.4. Identification of unknown DBPs

The fractions exhibiting significant toxic effects (>50 % inhibition of *P. phosphoreum* T3) were analyzed using an Agilent 1290 Infinity II liquid chromatograph coupled to an Agilent 6545 quadrupole time-of-flight mass spectrometer (LC-Q-TOF MS) (Singapore). An Agilent ZORBAX RRHD Eclipse Plus C18 column (2.1 × 150 mm × 1.8 μm) (the USA) maintained at 30 °C was used for separation. The mobile phases with a flow rate of 0.15 mL min^{-1} consisted of (A) water and (B) methanol, both containing 0.1 % formic acid. The injection volume was 10 μL. The Q-TOF MS, equipped with a dual jet stream electrospray ionization source, was operated in 2 GHz mode over a mass range of 50−1700 in negative polarity. The details of LC elution gradient and Q-TOF MS operation were provided in Text S9.

2.4. Computational methods

2.4.1. Theoretical calculation of phenoxyl radicals

The Gaussian 09 software package (the USA) was used to perform the theoretical calculations of the proposed phenoxyl radicals. The optimized geometry and frequency of each phenoxyl radical were calculated using DFT at the B3LYP/6–31G(d) level. Electron spin densities were calculated using DFT to quantify the degree of unpaired spins at various sites within radical species. The distribution of spin density was visualized in Table S7 using Multiwfn and Visual Molecular Dynamics (VMD) software.

2.4.2. Computational toxicity of halogenated coupling byproducts

The aquatic toxicity was assessed using the Ecological Structure Activity Relationships (ECOSAR) model (USEPA, 2020). Fish, daphnia, and green algae were selected as the target aquatic species to calculate the EC_{50} values that indicate acute toxicity.

To assess the potential human health effects, the inhibitory effects on thyroid hormones were examined using Danish QSAR database (Danish (Q)SAR, 2015; Rosenberg et al., 2016). The inhibitory effect on thyroperoxidase (TPO) was evaluated since it is the key enzyme for the synthesis of thyroid hormones. The Danish QSAR model predicts the probability (p) value between 0 and 1 for the ability of a tested compound to inhibit TPO activity. The approach of p value to 1 refers to the increase of likelihood of inhibiting TPO activity.

3. Results and discussion

3.1. Formation of known DBPs and TOX

The formation of six THMs, seven HALs, and nine HAAs was measured during UV/Chlorine reaction of phenol in the presence of Br^- or I^-. As illustrated in Fig. 1(a), THMs are the predominant DBPs, irrespective of the presence of I^-. The presence of Br^- slightly decreased the formation of trichloromethane (TCM) from 60 μg L^{-1} to 51 μg L^{-1}; however, it facilitated the formation of brominated THMs, including bromodichloromethane (BDCM), dibromochloromethane (DBCM), and tribromomethane (TBM). Additionally, the presence of Br^- imposed similar influences on the formation of HAAs compared to THMs. For example, the yields of trichloroacetic acid (TCAA) (23 μg L^{-1} and 24 μg L^{-1}) and dichloroacetic acid (DCAA) (7 μg L^{-1} and 9 μg L^{-1}) remains steady after involving Br^-. However, a significant amount of brominated HAAs was produced following the addition of Br^-, which even exceeded the amounts of chlorinated HAAs. Specifically, the amount of bromochloroacetic acid (BCAA) was the highest at 30 μg L^{-1}, followed by dibromoacetic acid (DBAA), dibromochloroacetic acid (DBCAA), and bromodichloroacetic acid (BDCAA). As for HALs, the presence of Br^- decreased the formation of CH from 7 μg L^{-1} to 4 μg L^{-1}, while increased the formation of DCAL (3 μg L^{-1}) and BDCAL (5 μg L^{-1}). Overall, the formation of known DBPs during UV/Chlorine reaction of phenol increased after the addition of Br^-. As previously reported, Br^- can be oxidized by chlorine to bromine ($HOBr/BrO^-$), especially under UV irradiation (Langsa et al., 2017; Soltermann et al., 2016). The generated $HOBr/BrO^-$ can halogenate phenol or Cl-DBPs to produce Br-DBPs, resulting in an increase in the DBP formation. The observed decrease in Cl-DBPs in the presence of Br^- is likely attributed to the consumption of Cl_2 by Br^- as well as the transformation of Cl-DBPs to Br-DBPs.

The addition of I^- exhibited negligible effects on the formation of known DBPs. Specifically, the addition of I^- was not observed to

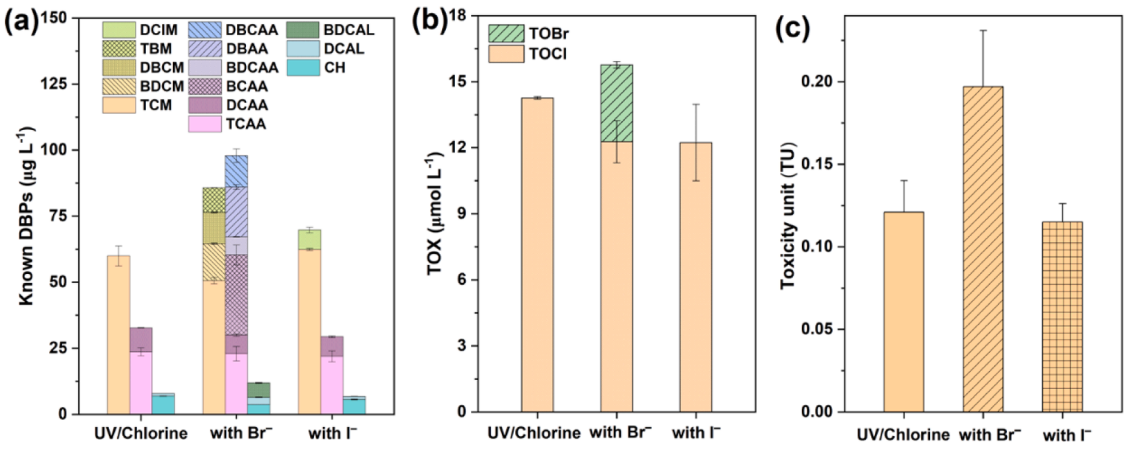

Fig. 1. (a) Known DBP formation, (b) TOX formation, and (c) Toxicity unit (TU=1/EC_{50}) of treated waters in UV/Chlorine reaction of phenol in presence of halides. Experiment conditions: $[Phenol]_0$ = 10 μM, $[Br^-]_0$ = 500 μg L^{-1}, $[I^-]_0$ = 100 μg L^{-1}, $[Cl_2]_0$ = 100 μM, UV fluence = 500 mJ cm^{-2}, pH = 7.

significantly alter the formation of TCM (62 μg L^{-1} and 60 μg L^{-1}, $p > 0.05$). In addition, I^- showed minimal effects on the formation of TCAA (22 μg L^{-1} and 24 μg L^{-1}), DCAA (8 μg L^{-1} and 9 μg L^{-1}), CH (7 μg L^{-1} and 6 μg L^{-1}) and DCAL (1 μg L^{-1} and 1 μg L^{-1}). Among the I-DBPs tested, only DCIM was detected at a concentration of 7 μg L^{-1}. Since I^- can be oxidized by Cl_2 to form active iodine (HOI/OI^-) followed by transformation to iodate, the generation of iodate was also analyzed (Hua et al., 2006; Mackeown et al., 2022). The results showed that in the UV/Chlorine reaction, over 50 % of the I^- was transformed into iodate (Fig. S1) (Hua et al., 2006), which explained the minimal effects of I^- addition on DBP yields.

The TOX formation was evaluated and the proportion of known DBPs was calculated. As shown in Fig. 1(b), the addition of Br^- increased the TOX formation (15.8 μmol L^{-1}) compared to that of without Br^- (14.3 μmol L^{-1}), in which TOCl accounted for 78 % and TOBr accounted for 22 %. To be more specific, Br^- decreased the TOCl formation from 14.3 μmol L^{-1} to 12.3 μmol L^{-1}, but resulted in the formation of TOBr (3.5 μmol L^{-1}). This can be ascribed to the consumption of chlorine in the generation of HOBr/BrO^- from Br^-, leading to the decreased formation of Cl-DBPs and increased formation of Br-DBPs. Besides, Br^- can also transform chlorine radicals ($Cl^•$, $ClO^•$, and $Cl_2^{•-}$) to bromine radicals ($Br^•$, $BrCl^•$, $BrO^•$, and $Br_2^{•-}$), which decreased the steady state concentrations of $HO^•$, $Cl^•$, and $Cl_2^{•-}$ from 1.73×10^{-14} M, 4.92×10^{-15} M, and 5.82×10^{-14} M to 1.54×10^{-14} M, 4.61×10^{-15} M, and 5.81×10^{-14} M, respectively. Chlorine radicals can react with NOM to form Cl-DBPs, while bromine radicals are unable to form Br-DBPs (Lei et al., 2022, 2021). Therefore, the decrease of Cl-DBP yields was observed along with the transformation of chlorine radicals to bromine radicals.

The addition of I^- decreased TOX formation from 14.3 μmol L^{-1} to12.8 μmol L^{-1}, which can also be attributed to the consumption of chlorine by I^-. Due to the relatively low I^- spiking concentration (0.79 μM) and the formation of iodate, the produced TOI is below detection limit (0.14 μM). Therefore, the addition of environmentally relevant concentration of I^- decreased the formation of TOCl, while produce minimal amounts of TOI, leading to a noticeable reduction in TOX formation. In general, the detected DBPs accounted only 16 %–21 % of TOX in terms of halogen per mole (Table S3), demonstrating that a large amount of DBPs remain unknown during the UV/Chlorine reaction in the presence of halides.

3.2. Identification of unknown DBPs

The treated water samples of UV/Chlorine reaction in presence of halides were subjected to toxicity assessment. In result, the addition of Br^- increased 63 % toxicity compared to the control set, while the addition of I^- was not observed to enhance the toxicity (Fig. 1(c)). This result was consistent with the formation of known DBPs and TOX. Therefore, the treated water of UV/Chlorine reaction in the presence of Br^- was selected for identification of unknown highly toxic DBPs by EDA. Before sample analysis, a series of model DBPs were tested to obtain the distribution of aliphatic and aromatic compounds during fractionation. In brief, aliphatic DBPs with LogKow ranging 0.34–1.44 occur in fractions F1–F4, while the aromatic DBPs with LogKow ranging 2.39–4.18 occur in fractions F5–F10. In the absence of Br^-, the distribution of TOX is presented in Fig. 2(a), in which F6 accounted for the largest proportion of TOX, followed by F5, F7, and F8. This result suggested that the halo-DBPs formed during UV/Chlorine reaction were mainly aromatic DBPs. On the other hand, F1, F5, F7, and F8 exhibited high toxicity, with >50 % cell luminescence inhibition rates (Fig. 2(b)). Noted that high toxicity but low TOX formation were obtained for F1, which was likely due to the presence of highly toxic non-halo aliphatic DBPs.

F1, F5, F7, and F8 showing high toxicity were selected for identification of unknown DBPs using LC-Q-TOF MS. In F1, the known DBPs such as DCAA and TCAA were detected, and three short-chain fatty acids were identified. The MS and MS/MS spectrum supported the identification of these three compounds as $C_4H_8O_5$ (2,3,4-trihydroxybutanoic acid), $C_5H_5ClO_5$ (2-chloro-3-oxopentanedioic acid), and $C_5H_8Cl_2O_6$ (2-chloro-3-(1-chloro-2-hydroxyethoxy)-2,3-dihydroxypropanoic acid), respectively (Fig. S5). Given six carbon atoms and four double bond equivalents (DBE), the aromatic DBPs in F5, F7, and F8 were screened accordingly (Table S5). Most of the detected compounds contain at least twelve carbon atoms with DBE≥8, which indicated that these compounds are dimers formed by coupling of two phenols. In result, the formulas of four halogenated coupling byproducts (P01–P04) were $C_{12}H_8Cl_2O_6$ (dichloro-hexahydroxy-biphenyl), $C_{12}H_9ClO_6$ (chloro-pentahydroxy-diphenyl ether), $C_{12}H_7Cl_3O_3$ (trichloro-dihydroxy-diphenyl ether), and $C_{12}H_7Cl_3O_3$ (trichloro-trihydroxy-biphenyl).

The addition of Br^- resulted in distinct differences in TOX and toxicity distributions. As presented in Fig. 2(c), F1 accounted for the largest proportion of TOX, followed by F6, F4, and F2. The increase of TOX proportion in F1–F4 indicated that more aliphatic halo-DBPs were produced with the addition of Br^-. This might be attributed to the formation of active bromine which decomposes aromatic compounds into aliphatic compounds (Criquet et al., 2015). F6–F9 showed relatively high toxicity (Fig. 2(d)), suggesting the formation of highly toxic aromatic DBPs. The identification results confirmed the presence of a series of coupling byproducts in these fractions. Following the same criteria (carbon atom amount and DBE values), four halogenated coupling byproducts (P05–P08) were identified and the formulas were

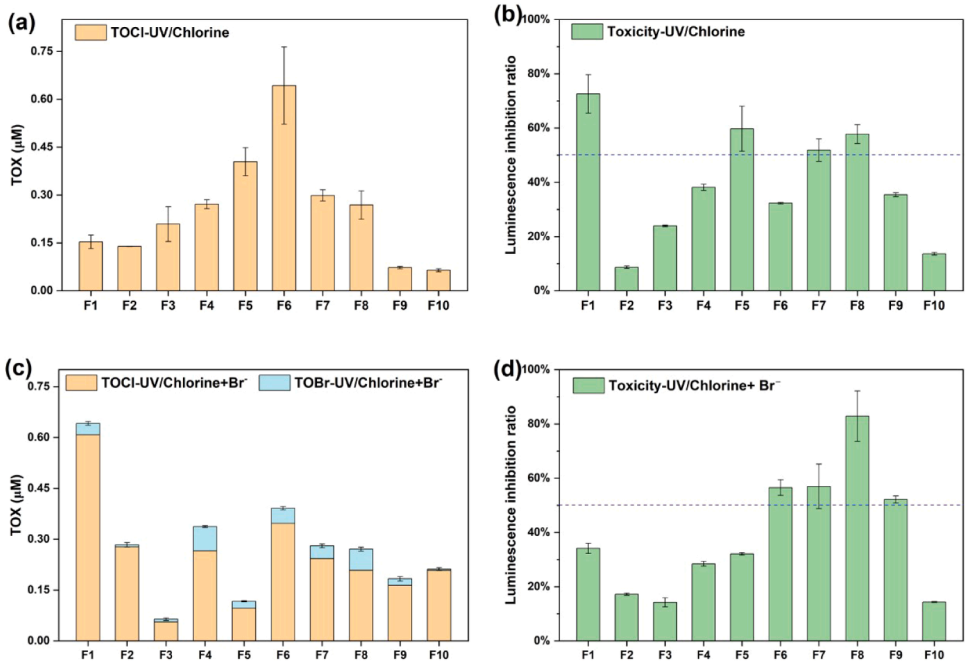

Fig. 2. (a) TOX formation and (b) toxicity of F1–F10 fractions of treated water in UV/Chlorine reaction of phenol. (c) TOX and (d) toxicity of F1-F10 fractions of treated water in UV/Chlorine reaction of phenol in presence of Br^-. Experiment conditions: $[Phenol]_0 = 10$ μM, $[Br^-]_0 = 500$ μg L^{-1}, $[I^-]_0 = 100$ μg L^{-1}, $[Cl_2]_0 = 100$ μM, UV fluence = 500 mJ $cm^{-2,}$ pH = 7, enrichment factor = 254.

$C_{12}H_7Cl_3O_2$ (trichloro-hydroxy-diphenyl ether), $C_{12}H_6BrCl_3O_2$ (bromo-trichloro-hydroxy-diphenyl ether), $C_{12}H_6Br_2Cl_2O_2$ (dibromo-dichloro-dihydroxy-diphenyl ether), and $C_{12}H_6Cl_4O_2$ (tetrachloro-hydroxy-diphenyl ether).

To further elucidate the structures of the halogenated coupling byproducts, the MS/MS features were combined with quantum chemical calculations to confirm the coupling bonds. Previous reports have indicated that the coupling reactions between phenoxyl radicals occur via the formation of carbon-carbon (C—C) bond or carbon-oxygen (C—O) bond (Carson and Kozlowski, 2024). Taken P03 ($C_{12}H_7Cl_3O_3$) as an example, its fragments include C_6H_4ClO and $C_6H_3Cl_2O_2$ (Fig. 3(b)), suggesting that P03 was generated from the coupling of $C_6H_4ClO^{\bullet}$ and $C_6H_3Cl_2O_2^{\bullet}$ via the formation of C—O bond. Meanwhile, computational calculations indicated that the high spin densities locate on O7, C3, C5 and C1 for $C_6H_4ClO^{\bullet}$, and O8, C1, and C5 for $C_6H_3Cl_2O_2^{\bullet}$ (Fig. 4). Considering the C_6H_4Cl fragment in the MS/MS spectrum (Fig. 3(b)), the oxygen atom in the C—O bond is presumed to originate from the hydroxy oxygen in $C_6H_4ClO^{\bullet}$. Although in $C_6H_3Cl_2O_2^{\bullet}$, C1 exhibited higher spin density than C5, C1 is occupied by the hydroxyl group, rendering coupling at C1 impossible. Therefore, O7 in $C_6H_4ClO^{\bullet}$ and C5 in $C_6H_3Cl_2O_2^{\bullet}$ were concluded as the bonding sites to form the P03 ($C_{12}H_7Cl_3O_3$). Similarly, the bonding sites of the other halogenated coupling byproducts were designated, which supported elucidating the structures of other halogenated coupling byproducts (Table S6). The

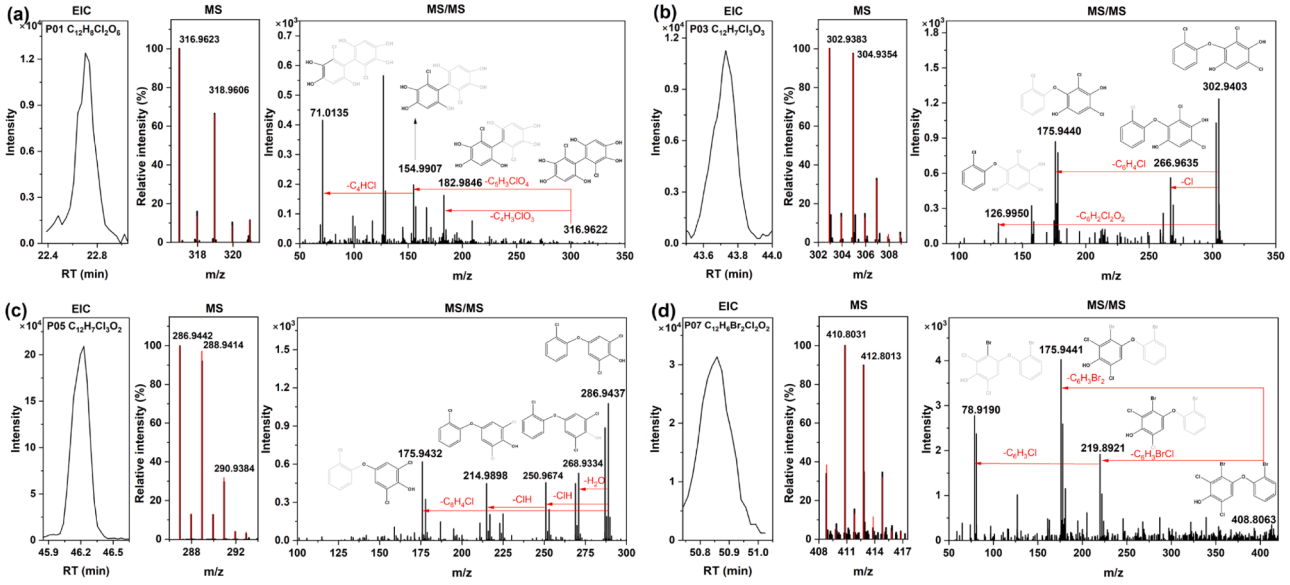

Fig. 3. EIC, MS spectra, and MS/MS spectra of (a) P01 $C_{12}H_8Cl_2O_6$, (b) P03 $C_{12}H_7Cl_3O_3$, (c) P05 $C_{12}H_7Cl_3O_2$, and (d) P07 $C_{12}H_6Br_2Cl_2O_2$. The MS spectra show the detected peaks (black) and the theoretical isotopic distributions of putatively identified compounds (red). The proposed structures and fragmentation pathways are shown in the MS/MS spectra.

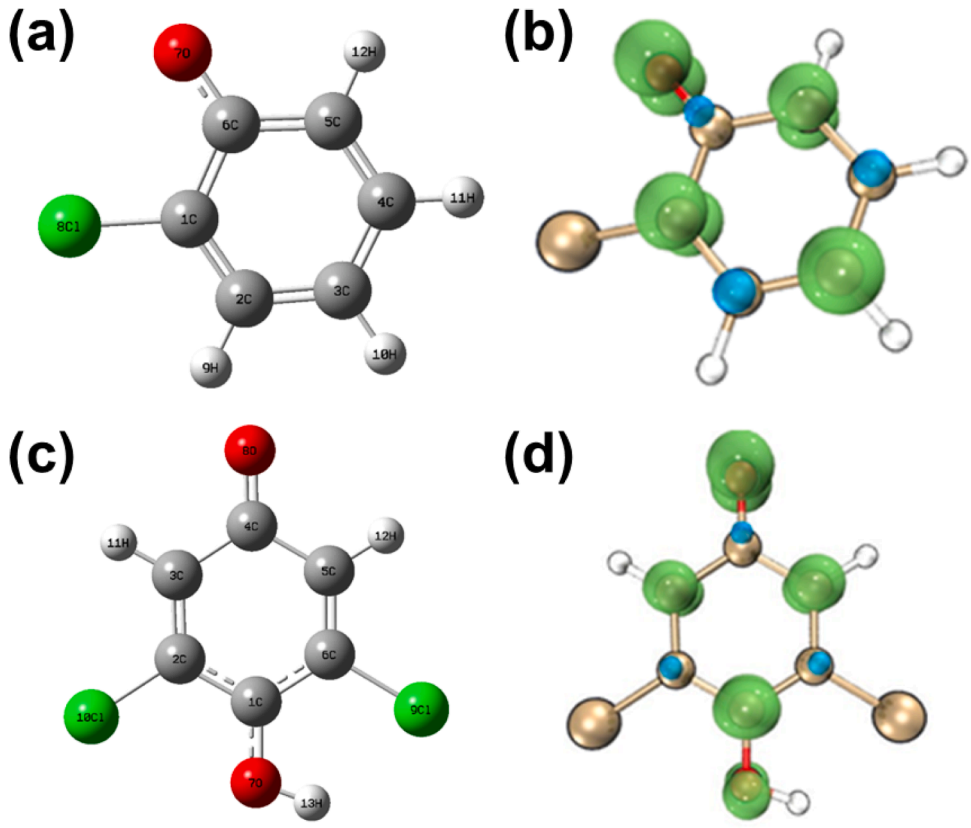

Fig. 4. (a) Lowest energy structure optimized by DFT and (b) isosurface map of the electron spin density of the $C_6H_4ClO^{\bullet}$ radical. (c) Lowest energy structure optimized by DFT and (d) isosurface map of the electron spin density of the $C_6H_3Cl_2O_2^{\bullet}$ radical. Noted that the halogenated coupling byproduct P03 are formed from these two phenoxyl radicals (green parts indicate positive values and blue parts indicate negative values).

halogenated coupling byproducts were confirmed in the simulated source water containing NOM after UV/Chlorine treatment. The formulas and structures of NOM-derived halogenated coupling byproducts (P09-P11) are presented in Table S6. Briefly, P09 ($C_{12}H_8Cl_2O_8$) was formed by coupling of two phenoxyl radicals, P10 ($C_{12}H_6Cl_2O_9$) was formed by coupling of a quinone radical and a phenoxyl radical, and P11 ($C_{12}H_5ClO_8$) was formed by coupling of two quinone radicals. The formation of P10 and P11 proceeds through coupling of quinone radicals generated from the oxidation of benzoquinone functional groups in NOM. A key distinction between UV/Chlorine-treated phenol and NOM systems lies in the structural complexity of NOM's functional groups, which leads to the production of more diverse transformation byproducts compared to those derived from phenol.

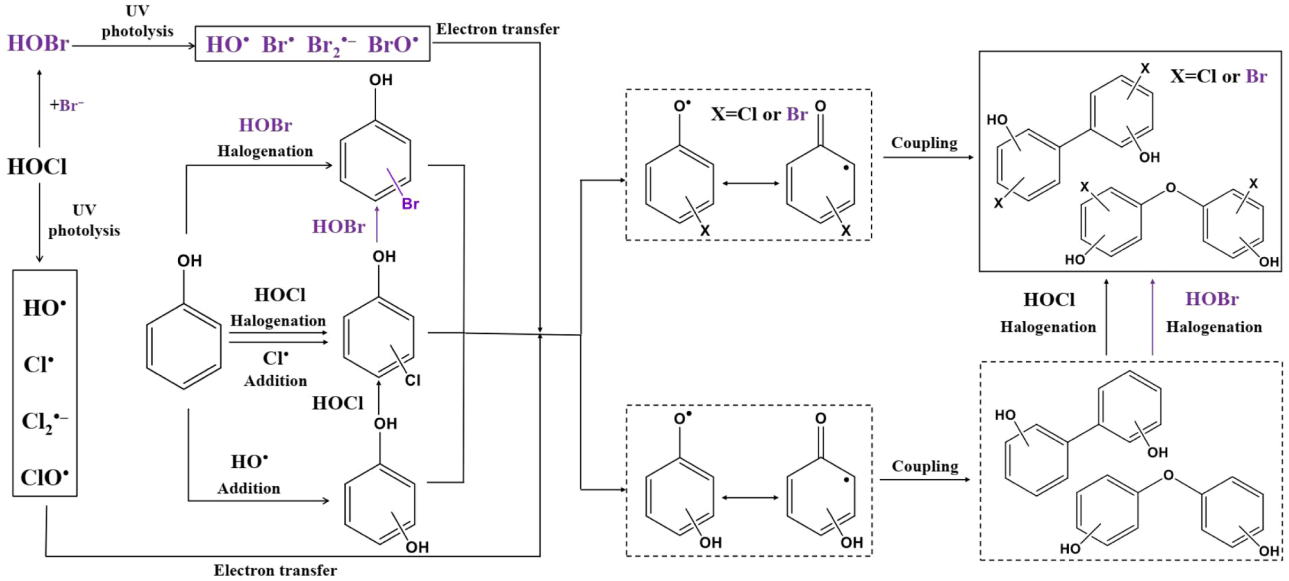

Fig. 5. Proposed formation pathways of halogenated coupling byproducts in UV/Chlorine reaction of phenol in presence of Br^-. Noted that the compounds in solid box have been identified while the ones in the dashed box are theoretically proposed (X = Cl or Br).

3.3. Formation mechanisms of halogenated coupling byproducts

Previous studies have demonstrated that aromatic radicals, such as phenoxyl radical, were crucial intermediates in the formation of coupling byproducts (Chen et al., 2024; Yang et al., 2023). Despite the widespread application of electron paramagnetic resonance (EPR) spectroscopy in radical detection, this analytical technique suffers from several inherent limitations, including relatively low sensitivity, susceptibility to matrix interference, and inability to provide molecular-level structural characterization of phenoxyl radicals. To circumvent these analytical constraints, complementary radical trapping approaches employing CHANT and TEMPO were implemented. As shown in Fig. S7, the phenoxyl radical ($C_6H_5O_3^{\bullet}$) was identified in the UV/Chlorine reaction of phenol, evidenced by the adducts with the specialized trapping agents CHANT and TEMPO. Having confirmed the generation of $C_6H_5O_3^{\bullet}$, the formation mechanisms of halogenated coupling byproducts in UV/Chlorine reaction of phenol were proposed based on HRMS analysis and quantum chemical calculations (Fig. 5). First, the phenoxyl radicals were generated through electron transfer reactions between phenolic compounds and radicals such as $HO^{\bullet}$, $Cl^{\bullet}$, and $Cl_2^{\bullet-}$ in UV/Chlorine reaction. Next, these phenoxyl radicals would couple to form coupling byproducts, followed by halogenation, hydroxylation, electrophilic aromatic substitution, and electron transfer. The halogenated coupling byproducts could be formed via another route, in which the phenolic compounds were substituted by chlorine or bromine to form halogenated phenols as well as by $HO^{\bullet}$ to form polyhydroxyl phenols. Next, the halogenated phenols and polyhydroxyl phenols were converted to phenoxyl radicals by free radicals ($HO^{\bullet}$, $Cl^{\bullet}$, $Cl_2^{\bullet-}$) through electron transfer reactions, and then reacted with each other to form halogenated coupling byproducts. Although both routes are theoretically feasible, the latter was less likely to occur due to the much higher reaction energy barriers in halogenation of coupling byproducts by chlorine or bromine (Li et al., 2022). To investigate the potential formation of halogenated coupling byproducts through chlorination alone, HRMS analysis was performed on chlorinated samples. The results revealed the detection of only one coupling product (P05), with an extracted ion chromatogram (EIC) peak intensity of approximately 0.7×10^4 (Fig. S8). This value was significantly lower than that observed in UV/Chlorine-treated samples (20×10^4), indicating that chlorination alone has limited efficacy in generating coupling byproducts. In contrast, UV/Chlorine treatment generates highly reactive inorganic radicals (e.g., $HO^{\bullet}$, $Cl^{\bullet}$, $ClO^{\bullet}$, and $Cl_2^{\bullet-}$), which substantially enhance phenoxyl radical production via electron transfer. Consequently, UV/Chlorine systems promote more efficient formation of coupling byproducts compared to chlorination.

3.4. Toxicity evaluation of halogenated coupling byproducts

The potential ecotoxicity and health risk of halogenated coupling byproducts were evaluated through computational analysis. As shown in Table 1, ECOSAR modelling results showed that the halogenated coupling byproducts exhibited higher ecotoxicity than phenol toward aquatic organisms such as fish, daphnia, and green algae. The toxicity patterns of halogenated coupling byproducts were similar to these of the low molecule weight DBPs. For example, the halogenated coupling byproducts containing quinones (P10 and P11) were found notably highly toxic, brominated coupling byproducts (P06 and P07) tended to be more toxic than the chlorinated ones, and the toxicity of chlorinated coupling byproducts increased with the increase of substituted chlorine atom numbers. While the predicted ecotoxicity for green algae was similar to that for fish, species related difference was noticed when compared to Daphnia. The quinoxyl coupling byproducts and brominated coupling byproducts were found to possess similar toxicity to the chlorinated ones, which might be ascribed to the distinct toxication mechanisms in Daphnia. Halogenated coupling byproducts demonstrated greater ecotoxicity compared to common aliphatic DBPs and aromatic DBPs. As detailed in Table S10, the LC_{50} values for fish exposure to halogenated coupling byproducts (0.11–32.3 mg L^{-1}) were substantially lower than those for aliphatic DBPs (25.8–2820.5 mg L^{-1}) and aromatic DBPs (2.3–13.7 mg L^{-1}). This enhanced toxicity pattern was consistently observed across daphnids and green algae test organisms, with the notable exception of HAAs in green algae exposure scenarios. The health risk of halogenated coupling byproducts was manifested as the inhibition on TPO activity. In general, the halogenated coupling byproducts exhibited enhanced inhibition with probability values>0.70. Noted that the halogenated coupling byproducts generated from NOM (P09–P11) possessed even higher probability (>0.88) of TPO inhibition.

Table 1
The predicted aquatic toxicity (mg L^{-1}) and thyroid interference of the halogenated coupling byproducts.

Compound	Fish LC_{50} (96 h)	Daphnid LC_{50} (48 h)	Green Algae EC_{50} (96 h)	Predicted probability of thyroperoxidase inhibition
Phenol	27.7	9.64	34.4	0.636
P01	13.6	100	5.88	0.993
P02	32.3	314	9.13	0.972
P03	0.82	2.70	1.17	0.703
P04	0.75	2.40	1.11	0.801
P05	0.26	0.61	0.61	0.492
P06	0.18	0.39	0.26	0.345
P07	0.14	0.33	0.20	0.345
P08	0.23	0.45	0.34	0.388
P09	5.00	5.00	6.40	0.973
P10	0.16	0.74	0.11	0.961
P11	0.11	0.45	0.09	0.883

4. Conclusions

As one of the commonly used AOPs, the DBP formation in UV/Chlorine reaction remains largely unknown. This study identified an important class of unknown DBPs, the halogenated coupling byproducts, in UV/Chlorine reaction of phenols in presence of halides. The EDA strategy enabled effective prioritization of the fractions possessing high toxicity, which facilitated the identification of highly toxic compounds. By combining HRMS analysis and theoretical computation, the structures of unknown halogenated coupling byproducts were concluded and their formation mechanisms were elucidated. Although coupling byproducts have been identified in chlorination and chloramination (Li et al., 2022; Wang et al., 2024; Xiang et al., 2020), this is the first study clarifying the formation of such high-molecule-weight DBPs in water disinfection by AOPs. While both chlorination and chloramination are capable of generating phenoxyl radicals and subsequent coupling byproducts, UV/Chlorine treatment enhanced byproduct formation through additional radical-mediated pathways. The photochemically generated reactive species (e.g., $HO^{\bullet}$, $Cl^{\bullet}$, and $Cl_2^{\bullet-}$) in UV/Chlorine treatment facilitate multiple parallel oxidation mechanisms that significantly increase the yield and diversity of coupling byproducts compared to conventional disinfection processes. The pervasive formation from NOM and the extraordinary toxic effects will certainly make halogenated coupling byproducts a significant concern in the future implementation of AOPs in water disinfection. Further efforts are suggested to measure the occurrence, concentration level, and actual toxicity of halogenated coupling byproducts formed from NOM in AOPs.

CRediT authorship contribution statement

Mengge Fan: Writing – original draft, Visualization, Validation, Software, Methodology, Investigation, Formal analysis, Data curation. **Yangjian Zhou:** Software, Formal analysis, Data curation. **Jialing Luo:** Software, Formal analysis. **Yanpeng Gao:** Software, Formal analysis.

Junlang Qiu: Writing – review & editing, Supervision, Resources, Funding acquisition, Conceptualization. **Xin Yang:** Writing – review & editing, Supervision, Resources, Funding acquisition, Conceptualization.

Declaration of competing interest

The authors declare that they have no known competing financial interests or personal relationships that could have appeared to influence the work reported in this paper.

Acknowledgements

This work was supported by the National Natural Science Foundation of China (42307308, 22376226, 22425607) and the National Key Research and Development Program of China (2023YFC3706700). The authors thank Ms. Haiyun Zhou (Instrumental Analysis and Research Center of Sun Yat-sen University) for the technical support on the mass spectrometry analysis.

Supplementary materials

Supplementary material associated with this article can be found, in the online version, at doi:10.1016/j.watres.2025.123981.

Data availability

Data will be made available on request.

References

Alexandrou, L., Meehan, B.J., Jones, O.a.H., 2018. Regulated and emerging disinfection by-products in recycled waters. Sci. Total. Environ. 637–638, 1607–1616.
Allen, J.M., Plewa, M.J., Wagner, E.D., Wei, X., Bokenkamp, K., Hur, K., Jia, A., Liberatore, H.K., Lee, C.-F.T., Shirkhani, R., Krasner, S.W., Richardson, S.D., 2022a. Drivers of disinfection byproduct cytotoxicity in U.S. drinking water: should other DBPs be considered for regulation? Env. Sci. Technol. 56 (1), 392–402.
Allen, J.M., Plewa, M.J., Wagner, E.D., Wei, X., Bokenkamp, K., Hur, K., Jia, A., Liberatore, H.K., Lee, C.-F.T., Shirkhani, R., Krasner, S.W., Richardson, S.D., 2022b. Feel the burn: disinfection byproduct formation and cytotoxicity during chlorine burn events. Env. Sci. Technol. 56 (12), 8245–8254.
Bolton, J.R., Stefan, M.I., Shaw, P.-S., Lykke, K.R., 2011. Determination of the quantum yields of the potassium ferrioxalate and potassium iodide–iodate actinometers and a method for the calibration of radiometer detectors. J. Photochem. Photobiol. A: Chem. 222 (1), 166–169.
Brack, W., 2003. Effect-directed analysis: a promising tool for the identification of organic toxicants in complex mixtures? Anal. Bioanal. Chem. 377 (3), 397–407.
Brack, W., Ait-Aissa, S., Burgess, R.M., Busch, W., Creusot, N., Di Paolo, C., Escher, B.I., Mark Hewitt, L., Hilscherova, K., Hollender, J., Hollert, H., Jonker, W., Kool, J., Lamoree, M., Muschket, M., Neumann, S., Rostkowski, P., Ruttkies, C., Schollee, J., Schymanski, E.L., Schulze, T., Seiler, T.-B., Tindall, A.J., De Aragão Umbuzeiro, G., Vrana, B., Krauss, M., 2016. Effect-directed analysis supporting monitoring of aquatic environments — An in-depth overview. Sci. Total. Environ. 544, 1073–1118.
Bulman, D.M., Milstead, R.P., Remucal, C.K., 2023. Formation of targeted and novel disinfection byproducts during chlorine photolysis in the presence of bromide. Env. Sci. Technol. 57 (47), 18877–18887.
Carson, M.C., Kozlowski, M.C., 2024. Recent advances in oxidative phenol coupling for the total synthesis of natural products. Nat. Prod. Rep. 41 (2), 208–227.
Chen, C., Zhao, X., Chen, H., Li, Z., Ma, B., Wang, Y., Xian, Q., 2025. Generation of DBPs from dissolved organic matter by solar photolysis of chlorine: associated changes of cytotoxicity and reactive species. Water. Res. 274, 123074.
Chen, Y.-D., Duan, X., Zhou, X., Wang, R., Wang, S., Ren, N.-Q., Ho, S.-H., 2021. Advanced oxidation processes for water disinfection: features, mechanisms and prospects. Chem. Eng. J. 409, 128207.
Chen, Y., Ren, W., Ma, T., Ren, N., Wang, S., Duan, X., 2024. Transformative removal of aqueous micropollutants into polymeric products by advanced oxidation processes. Env. Sci. Technol. 58 (11), 4844–4851.
Cheng, S., Zhang, X., Yang, X., Shang, C., Song, W., Fang, J., Pan, Y., 2018. The multiple role of bromide ion in PPCPs degradation under UV/chlorine treatment. Env. Sci. Technol. 52 (4), 1806–1816.
Criquet, J., Rodriguez, E.M., Allard, S., Wellauer, S., Salhi, E., Joll, C.A., Von Gunten, U., 2015. Reaction of bromine and chlorine with phenolic compounds and natural organic matter extracts – Electrophilic aromatic substitution and oxidation. Water. Res. 85, 476–486.
Danish(Q)SAR (2015), http://qsar.food.dtu.dk/.
Dong, F., Lin, Q., Li, C., Wang, L., García, A., 2021. UV/chlorination process of algal-laden water: algal inactivation and disinfection byproducts attenuation. Sep. Purif. Technol. 257, 117896.
Dong, H., Cuthbertson, A.A., Plewa, M.J., Weisbrod, C.R., Mckenna, A.M., Richardson, S. D., 2023. Unravelling High-Molecular-Weight DBP Toxicity Drivers in Chlorinated and Chloraminated Drinking Water: Effect-Directed Analysis of Molecular Weight Fractions. Environ. Sci. Technol. 18788–18800.
Dong, H., Cuthbertson, A.A., Richardson, S.D., 2020. Effect-directed analysis (EDA): a promising tool for nontarget identification of unknown disinfection byproducts in drinking water. Env. Sci. Technol. 54 (3), 1290–1292.
Fan, M., Yang, X., Kong, Q., Lei, Y., Zhang, X., Aghdam, E., Yin, R., Shang, C., 2022. Sequential ClO_2-UV/chlorine process for micropollutant removal and disinfection byproduct control. Sci. Total. Environ. 806, 150354.
Gao, Z.-C., Lin, Y.-L., Xu, B., Xia, Y., Hu, C.-Y., Zhang, T.-Y., Qian, H., Cao, T.-C., Gao, N.-Y., 2020. Effect of bromide and iodide on halogenated by-product formation from different organic precursors during UV/chlorine processes. Water. Res. 182, 116035.
Hua, G., Reckhow, D.A., Kim, J., 2006. Effect of bromide and iodide ions on the formation and speciation of disinfection byproducts during chlorination. Env. Sci. Technol. 40 (9), 3050–3056.
Huang, J., Wu, Y., Wu, Y., Sheng, D., Sun, J., Bu, L., Zhou, S., 2022. Comparison of UV and UV/chlorine system on degradation of 2,4-diaminobutyric acid and formation of disinfection byproducts in subsequent chlorination. Sep. Purif. Technol. 284, 120264.
Jiang, Y., Zang, S., Qiao, Y., Tan, Y., Tao, H., Li, Q., Ma, Y., Wang, X., Ma, J., 2025. Occurrence, toxicity, and control of halogenated aliphatic and phenolic disinfection byproducts in the chlorinated and chloraminated desalinated water. Water. Res. 268, 122566.
Kong, Q., Ye, L., Pan, Y., Zhou, Y., Lei, Y., Zeng, Z., Chen, S., Yao, L., Zhang, X., Westerhoff, P., Yang, X., 2023. Photochemical transformation of free chlorine induced by triplet state dissolved organic matter. Env. Sci. Technol. 57 (29), 10849–10859.
Langsa, M., Heitz, A., Joll, C.A., Von Gunten, U., Allard, S., 2017. Mechanistic aspects of the formation of adsorbable organic bromine during chlorination of bromide-containing synthetic waters. Env. Sci. Technol. 51 (9), 5146–5155.
Lavonen, E.E., Gonsior, M., Tranvik, L.J., Schmitt-Kopplin, P., Köhler, S.J., 2013. Selective chlorination of natural organic matter: identification of previously unknown disinfection byproducts. Env. Sci. Technol. 47 (5), 2264–2271.
Lei, Y., Cheng, S., Luo, N., Yang, X., An, T., 2019. Rate constants and mechanisms of the reactions of $Cl^{\bullet}$ and $Cl_2^{\bullet-}$ with trace organic contaminants. Env. Sci. Technol. 53 (19), 11170–11182.
Lei, Y., Lei, X., Westerhoff, P., Tong, X., Ren, J., Zhou, Y., Cheng, S., Ouyang, G., Yang, X., 2022. Bromine radical ($Br^{\bullet}$ and $Br_2^{\bullet-}$) reactivity with dissolved organic matter and brominated organic byproduct formation. Env. Sci. Technol. 56 (8), 5189–5199.
Lei, Y., Lei, X., Westerhoff, P., Zhang, X., Yang, X., 2021. Reactivity of chlorine radicals ($Cl^{\bullet}$ and $Cl_2^{\bullet-}$) with dissolved organic matter and the formation of chlorinated byproducts. Env. Sci. Technol. 55 (1), 689–699.
Li, D., Yang, X., Zhou, Z., Jiang, B., Tawfik, A., Zhao, S., Meng, F., 2019. Molecular traits of phenolic moieties in dissolved organic matter: linkages with membrane fouling development. Env. Int. 133, 105202.
Li, W., Zhang, X., Han, J., 2022. Formation of larger molecular weight disinfection byproducts from acetaminophen in chlorine disinfection. Env. Sci. Technol. 56 (23), 16929–16939.
Li, X.-F., Mitch, W.A., 2018. Drinking water disinfection byproducts (DBPs) and human health effects: multidisciplinary challenges and opportunities. Env. Sci. Technol. 52 (4), 1681–1689.
Liu, C., Ersan, M.S., Plewa, M.J., Amy, G., Karanfil, T., 2019. Formation of iodinated trihalomethanes and noniodinated disinfection byproducts during chloramination of algal organic matter extracted from Microcystis aeruginosa. Water. Res. 162, 115–126.
Liu, C., Shin, Y.-H., Wei, X., Ersan, M.S., Wagner, E., Plewa, M.J., Amy, G., Karanfil, T., 2022. Preferential halogenation of algal organic matter by iodine over chlorine and bromine: formation of disinfection byproducts and correlation with toxicity of disinfected waters. Env. Sci. Technol. 56 (2), 1244–1256.
Liu, S., Li, Z., Dong, H., Goodman, B.A., Qiang, Z., 2017. Formation of iodo-trihalomethanes, iodo-acetic acids, and iodo-acetamides during chloramination of iodide-containing waters: factors influencing formation and reaction pathways. J. Hazard. Mater. 321, 28–36.
Liu, Z.-Q., Shah, A.D., Salhi, E., Bolotin, J., Von Gunten, U., 2018. Formation of brominated trihalomethanes during chlorination or ozonation of natural organic matter extracts and model compounds in saline water. Water. Res. 143, 492–502.
Mackeown, H., Von Gunten, U., Criquet, J., 2022. Iodide sources in the aquatic environment and its fate during oxidative water treatment – A critical review. Water. Res. 217, 118417.
Mitch, W.A., Richardson, S.D., Zhang, X., Gonsior, M., 2023. High-molecular-weight by-products of chlorine disinfection. Nat. Water 1 (4), 336–347.
Qian, Y., Chen, Y., Hu, Y., Hanigan, D., Westerhoff, P., An, D., 2021. Formation and control of C- and N-DBPs during disinfection of filter backwash and sedimentation sludge water in drinking water treatment. Water. Res. 194, 116964.
Rahn, R., 1997. Potassium iodide as a chemical actinometer for 254 nm radiation: use of iodate as an electron scavenger. Photochem. Photobiol. 66 (4), 450–455.
Rosenberg, S.A., Nikolov, N.G., Dybdahl, M., Simmons, S., Crofton, K.M., Watt, E.D., Friedmann, K.P., Judson, R.S., Wedebye, E.B., 2016. Development of a QSAR Model for thyroperoxidase inhibition and screening of 72,526. Reach. Subst.
Shimabuku, K., Henrie, T., Schultise, D., Pillai, S., 2024. Modeling chloramine stability and disinfection byproduct formation in groundwater high in bromide. AWWa Water. Sci. 6 (1), e1365.

Soltermann, F., Abegglen, C., Gotz, C., Von Gunten, U., 2016. Bromide sources and loads in Swiss surface waters and their relevance for bromate formation during wastewater ozonation. Env. Sci. Technol. 50 (18), 9825–9834.
Srivastav, A.L., Patel, N., Chaudhary, V.K., 2020. Disinfection by-products in drinking water: occurrence, toxicity and abatement. Environ. Pollut. 267, 115474.
USEPA, 2020. ECOSAR. United States Environmental Protection Agency. https://www.epa.gov/tsca-screening-tools/ecological-structure-activity-relationships-ecosar-predictive-model.
Wang, P., Ye, B., Nomura, Y., Fujiwara, T., 2024. Revisiting the chloramination of phenolic compounds: formation of novel high-molecular-weight nitrogenous disinfection byproducts. Water. Res. 266, 122335.
Wang, W.-L., Zhang, X., Wu, Q.-Y., Du, Y., Hu, H.-Y., 2017. Degradation of natural organic matter by UV/chlorine oxidation: molecular decomposition, formation of oxidation byproducts and cytotoxicity. Water. Res. 124, 251–258.
Wang, Y., Le Roux, J., Zhang, T., Croué, J.-P., 2014. Formation of brominated disinfection byproducts from natural organic matter isolates and model compounds in a sulfate radical-based oxidation process. Env. Sci. Technol. 48 (24), 14534–14542.
Watson, K., Farré, M.J., Leusch, F.D.L., Knight, N., 2018. Using fluorescence-parallel factor analysis for assessing disinfection by-product formation and natural organic matter removal efficiency in secondary treated synthetic drinking waters. Sci. Total. Environ. 640, 31–40.
Xiang, W., Qu, R., Wang, X., Wang, Z., Bin-Jumah, M., Allam, A.A., Zhu, F., Huo, Z., 2020. Removal of 4-chlorophenol, bisphenol A and nonylphenol mixtures by aqueous chlorination and formation of coupling products. Chem. Eng. J. 402, 126140.
Yang, S.-Q., Liu, Z.-Q., Cui, Y.-H., Wang, M.-K., 2023. Organics abatement and recovery from wastewater by a polymerization-based electrochemically assisted persulfate process: promotion effect of chloride ion and its mechanism. J. Hazard. Mater. 446, 130658.
Yang, W., Guo, J., Hee, S., Chen, Y., 2025. Recent advances in iodine-mediated radical reactions. Adv. Synth. Catal. 367 (7), e202401486.
Yang, Y., Komaki, Y., Kimura, S.Y., Hu, H.-Y., Wagner, E.D., Mariñas, B.J., Plewa, M.J., 2014. Toxic impact of bromide and iodide on drinking water disinfected with chlorine or chloramines. Env. Sci. Technol. 48 (20), 12362–12369.
Ye, T., Zhang, T.-Y., Tian, F.-X., Xu, B., 2021. The fate and transformation of iodine species in UV irradiation and UV-based advanced oxidation processes. Water. Res. 206, 117755.
Yeom, Y., Han, J., Zhang, X., Shang, C., Zhang, T., Li, X., Duan, X., Dionysiou, D.D., 2021. A review on the degradation efficiency, DBP formation, and toxicity variation in the UV/chlorine treatment of micropollutants. Chem. Eng. J. 424, 130053.
Zhang, S., Wei, J., Wu, N., Allam, A.A., Ajarem, J.S., Maodaa, S., Huo, Z., Zhu, F., Qu, R., 2024. Assessment of the UV/DCCNa and UV/NaClO oxidation process for the removal of diethyl phthalate (DEP) in the aqueous system. Environ. Pollut. 341, 122915.
Zhang, S.N., Wei, J.Y., Guo, R.X., Liu, B.Y., Qu, R.J., Huo, Z.L., Zhu, F., 2023. The transformation and interaction of diallyl phthalate (DAP) in the three kinds of plastic under ultraviolet/sodium dichloroisocyanurate (UV/DCCNa) disinfection process. Chem. Eng. J. 467.
Zhang, X., Guo, K., Wang, Y., Qin, Q., Yuan, Z., He, J., Chen, C., Wu, Z., Fang, J., 2020. Roles of bromine radicals, HOBr and Br_2 in the transformation of flumequine by the UV/chlorine process in the presence of bromide. Chem. Eng. J. 400, 125222.
Zhao, X., Chen, C., Chen, H., Guo, Y., Zhang, X., Li, M., Cao, L., Wang, Y., Gong, T., Che, L., Yang, G., Xian, Q., 2023. Evolutions of dissolved organic matter and disinfection by-products formation in source water during UV-LED (275 nm)/chlorine process. Water Res. 243, 120284.
Zheng, S., Ji, H., Qin, W., Chen, C., Wu, Z., Guo, K., Wei, W., Guo, W., Fang, J., 2023. Production of reactive species during UV photolysis of chlorite for the transformation of micropollutants in simulated drinking water. Chem. Eng. J. 470, 144076.
Zhong, Y., Gan, W., Du, Y., Huang, H., Wu, Q., Xiang, Y., Shang, C., Yang, X., 2019. Disinfection byproducts and their toxicity in wastewater effluents treated by the mixing oxidant of ClO_2/Cl_2. Water. Res. 162, 471–481.